Environmental Science & Technology
pubs.acs.org/est
Article

No Evidence for a Significant Impact of Heterogeneous Chemistry on Radical Concentrations in the North China Plain in Summer 2014

Zhaofeng Tan, Andreas Hofzumahaus, Keding Lu, Steven S. Brown, Frank Holland, Lewis Gregory Huey, Astrid Kiendler-Scharr, Xin Li, Xiaoxi Liu, Nan Ma, Kyung-Eun Min, Franz Rohrer, Min Shao, Andreas Wahner, Yuhang Wang, Alfred Wiedensohler, Yusheng Wu, Zhijun Wu, Limin Zeng, Yuanhang Zhang, and Hendrik Fuchs*

Cite This: *Environ. Sci. Technol.* 2020, 54, 5973−5979

Read Online

ACCESS | Metrics & More | Article Recommendations | Supporting Information

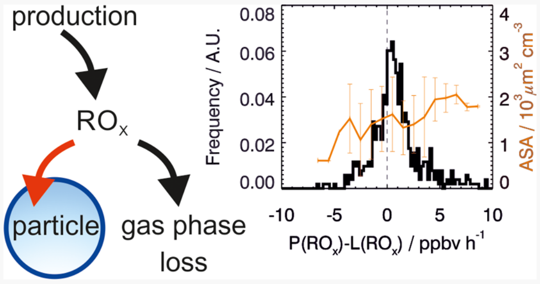

ABSTRACT: The oxidation of nitric oxide to nitrogen dioxide by hydroperoxy (HO_2) and organic peroxy radicals (RO_2) is responsible for the chemical net ozone production in the troposphere and for the regeneration of hydroxyl radicals, the most important oxidant in the atmosphere. In Summer 2014, a field campaign was conducted in the North China Plain, where increasingly severe ozone pollution has been experienced in the last years. Chemical conditions in the campaign were representative for this area. Radical and trace gas concentrations were measured, allowing for calculating the turnover rates of gas-phase radical reactions. Therefore, the importance of heterogeneous HO_2 uptake on aerosol could be experimentally determined. HO_2 uptake could have suppressed ozone formation at that time because of the competition with gas-phase reactions that produce ozone. The successful reduction of the aerosol load in the North China Plain in the last years could have led to a significant decrease of HO_2 loss on particles, so that ozone-forming reactions could have gained importance in the last years. However, the analysis of the measured radical budget in this campaign shows that HO_2 aerosol uptake did not impact radical chemistry for chemical conditions in 2014. Therefore, reduced HO_2 uptake on aerosol since then is likely not the reason for the increasing number of ozone pollution events in the North China Plain, contradicting conclusions made from model calculations reported in the literature.

1. INTRODUCTION

In the last years, ozone (O_3) pollution has become a major concern in China because of an increasing number of high ozone concentration events.[1−5] The only relevant chemical source of tropospheric O_3 is the oxidation of nitric oxide (NO) to nitrogen dioxide (NO_2) by hydroperoxy (HO_2) and organic peroxy (RO_2) radicals. Ozone is then produced from the photolysis of NO_2.

Several reasons have been suggested to explain the increase in the number of high ozone pollution events. The global O_3 background concentration increased[6−8] and meteorological conditions (e.g., high temperature or more sunlight) could have favored ozone pollution.[9,10] Regulations in China focused on limiting nitrogen oxide ($NO_x = NO_2 + NO$) emissions but neglected volatile organic compound emissions. This change in the mix of anthropogenic emissions could contribute to increasing ozone concentrations[11−13] because it could have shifted the chemical regime from conditions in which ozone production is suppressed by nitrogen oxides to conditions in which the oxidation of organic compounds leads to efficient ozone production.[14−17] A recent modeling study attributed the increase in ozone concentrations in China between 2014 and 2017 mainly to the significant reduction of particle concentrations, as suggested by Li et al.[1] The mechanism behind this would be that heterogeneous HO_2 radical loss on aerosol suppressed ozone formation. Cleaning the air from aerosol would result in higher HO_2 concentrations and consequently in higher ozone production. The increase in radical production due to higher actinic flux would play only a minor role.[1]

The reaction of HO_2 with NO is not only responsible for photochemical ozone formation but is also important for the regeneration of hydroxyl radicals (OH), the most important gas-phase oxidant during daytime. Therefore, the competition between gas-phase HO_2 loss by NO and heterogeneous HO_2 loss on particles also impacts the oxidation capacity in continental areas dominated by anthropogenic emissions.

Received: January 27, 2020
Revised: April 27, 2020
Accepted: April 28, 2020
Published: April 28, 2020

https://dx.doi.org/10.1021/acs.est.0c00525
Environ. Sci. Technol. 2020, 54, 5973−5979

For small particles (submicrometer), the heterogeneous loss rate is not limited by gas-phase diffusion but by the transfer through the gas/particle interface.[18] The latter is described by eq 1.

$$L(HO_2)_{het} = 0.25 \cdot \gamma_{eff} \cdot \nu_{HO_2} \cdot ASA \cdot [HO_2] \quad (1)$$

The rate is proportional to the aerosol surface area (ASA) concentration and the mean molecular velocity of HO_2 (ν_{HO_2}, e.g. 4.44×10^5 cm/s at 25 °C). The effective uptake coefficient γ_{eff} parametrizes the influence of processes such as rebouncing when HO_2 hits the surface, evaporation into the gas phase, and diffusion and chemical reaction in the particle.

HO_2 uptake on the aqueous aerosol surface is facilitated by its high solubility and capability to dissociate to H^+ and O_2^- in water.[18] The presence of dissolved transition metal ions (TMIs) in the aerosol catalyzes the conversion of HO_2 to oxidation products and thus increases the uptake flux.[19−22] In contrast, organic coating of aerosol can inhibit the reactive uptake.[23,24] Laboratory studies using artificial aerosol give effective uptake coefficients ranging from 10^{-5} to unity depending on the aerosol chemical composition and its mixing state.[21−28] So far, the uptake coefficient has only been measured once for real aerosol from the North China Plain.[20] The relatively high value of 0.2 is likely due to the abundance of dissolved copper ions Cu(I)/Cu(II) in aqueous aerosol. In the model studies by Li et al.,[1,2] this high value is applied for all conditions in China between 2014 and 2017.

In this study, measurements from a field campaign during summertime in the North China Plain,[29,30] where a significant ozone increase from 80 ppbv to more than 100 ppbv was observed between 2014 and 2018 (Figure S2), are used to calculate turnover rates of gas-phase radical reactions resulting in ozone production. Because ozone formation is connected to photochemistry, the analysis is done under daytime conditions, and nighttime chemistry is not further discussed in this work. The campaign was conducted shortly after the Clean Air Action Plan of the Chinese government was put into force in 2013. Therefore, particulate matter pollution was still high (60 μg/m^3 average during the campaign) and thus, the impact of aerosol uptake could have been an important radical loss.

2. FIELD MEASUREMENT AND METHODS

The field campaign aimed to investigate the role of radical chemistry in air pollution formation in the North China Plain. A comprehensive suite of instruments detecting gas-phase species and characterizing particle properties were deployed. For the analysis here, measurements of concentrations of radicals (OH, HO_2, and RO_2), ozone, nitrous acid (HONO), formaldehyde (HCHO), nitryl chloride ($ClNO_2$), molecular chloride (Cl_2), and aerosol surface area (ASA) and the measurement of the total OH radical loss rate (OH reactivity = inverse lifetime of OH) are used (Table S2). Details of the field site and instrumentation can be found in previous publications.[29−33]

In the previous analysis of the radical chemistry, it was shown that OH production and destruction rates determined from measured gas-phase species were balanced.[30] This indicates that OH loss and production can be explained by known radical chemistry reactions. Approximately 40% of the total OH loss was due to reactions with inorganic species (NO_x and CO) and the remaining fraction due to organic compounds. The sum of measured OH reactant concentrations matched the observed OH reactivity, demonstrating that all important OH reactants were detected.[30]

Because of the short chemical lifetime of radicals (typically less than a minute), their concentrations are expected to be in a steady state, with production and destruction rates balanced. The turnover rates of gas-phase production and destruction rates that were important for the HO_2 and RO_x (=RO_2 + HO_2 + OH) radical budgets during the campaign (Figure 1) can be calculated from measured trace gases, radicals, and photolysis frequencies (Supporting Information). If heterogeneous HO_2 loss had been a significant loss process, an imbalance between production and destruction rates would be expected, if only gas-phase reactions are taken into account.

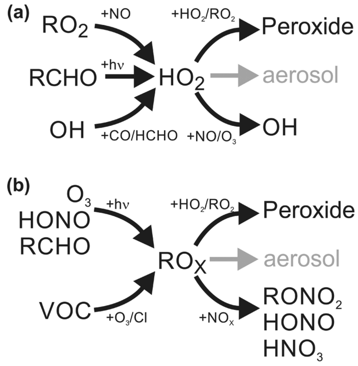

Figure 1. Schematics of (a) HO_2 and (b) RO_x (OH + HO_2 + RO_2) loss and production processes.

Gas-phase radical production and destruction reactions can be distinguished by their roles for the radical budgets.[36] Radical production reactions from nonradical precursors (primary sources) lead to an increase of the total RO_x radical concentration, and radical recombination reactions act as permanent sinks for RO_x. In contrast, reactions in which the number of consumed and produced radicals is equal do not change the total RO_x concentration. As a consequence, radical conversion reactions cancel out in the RO_x radical budget, whereas the HO_2 budget contains all types of radical reactions.

Total radical (RO_x) primary production includes ozonolysis of alkenes, the reaction of chlorine atoms (Cl) with organic compounds, photolysis of HONO, photolysis of O_3 with subsequent reaction with water, and photolysis of carbonyl-containing species (eq S3, Supporting Information). RO_x termination processes are reactions between OH and NO_x, radical recombination reactions between HO_2 and RO_2, and nitrate formation from reactions of RO_2 radicals with NO (eq S4, Supporting Information).

The production of HO_2 consists of several primary sources, mainly photolysis of molecules containing a carbonyl group (RCHO), most importantly formaldehyde, and ozonolysis of alkenes (Figure 1). In addition, HO_2 is formed in radical chain propagation reactions from either OH with mainly CO or formaldehyde or from reactions of RO_2 radicals with NO (eq S1, Supporting Information). Gas-phase HO_2 destruction includes radical recombination reactions with other peroxy radicals (HO_2 and RO_2), forming peroxides, and the reaction with NO. Potential loss due to heterogeneous uptake on the aerosol surface would add to the gas-phase loss (eq S2, Supporting Information).

3. RESULTS AND DISCUSSION

Photolysis reactions of ozone, nitrous acid, and carbonyl compounds are the most important contributors (62%) to primary radical production during daytime and therefore, the calculated RO_x production rate peaks with values of up to 12 ppbv/h around noontime, when solar radiation is the strongest (Figures 2 and S3). Photolysis of $ClNO_2$ or Cl_2 (reactions S21 and S22, Supporting Information) is a source for Cl atoms. Measurements of $ClNO_2$ and Cl_2 concentrations during this campaign gave on average concentrations of 1 ppbv and 100 pptv, respectively (Figure S4). Assuming that each Cl atom results in one RO_2 radical (reaction S20, Supporting Information), an averaged production rate of 1.7 ppbv/h during daytime is obtained.[33] This value is included as an upper limit for the production of RO_x radicals from Cl atoms in the budget analysis, which increases the total radical production compared to a previous model-based study.[29] Another contribution to $P(RO_x)$ comes from the ozonolysis of alkenes with a value of 0.5 ppb/h (Figure 3a).

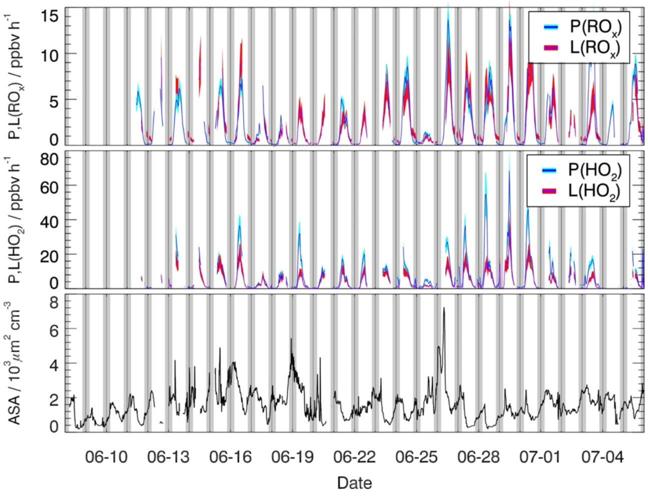

Figure 2. Time series of RO_x and HO_2 loss and production rates and of ASA concentration during the campaign. Colored areas denote the uncertainty in the experimental budget calculation (see text) and grey areas denote nighttime.

On average, the total radical (RO_x) production is balanced by gas-phase radical loss reactions, mainly from the reactions with NO_x and radical self-reactions. Only an insignificant discrepancy of 0.6 ± 1.3 ppbv/h remains (Figures 3a and 4). The leading uncertainties of the calculated destruction rates are the accuracies in the yields of nitrates from the reaction of RO_2 with NO and in the $HO_2 + RO_2$ reaction rate constants, which depend on the exact RO_2 speciation that is not known (Supporting Information). A lower limit for a nitrate yield of 5% is assumed for all RO_2. Higher yields that could be up to 30% for specific RO_2 would bring $P(RO_x)$ and $L(RO_x)$ in even better agreement but cannot balance radical loss by HO_2 uptake on aerosol. Results would not change if the nitrate yield was higher (Figure S8). The $HO_2 + RO_2$ reaction (reaction S2) rate constants for different RO_2 species vary typically within 30% but can also be as high as a factor of 4.[37] For example, changing the value of 1.7×10^{-11} cm^{-3} s^{-1} (298 K) used in the calculations within this range (30%) doubles the imbalance in the RO_x budget to 1.2 ppbv/h. These uncertainties demonstrate that there is no significant imbalance in the RO_x budget.

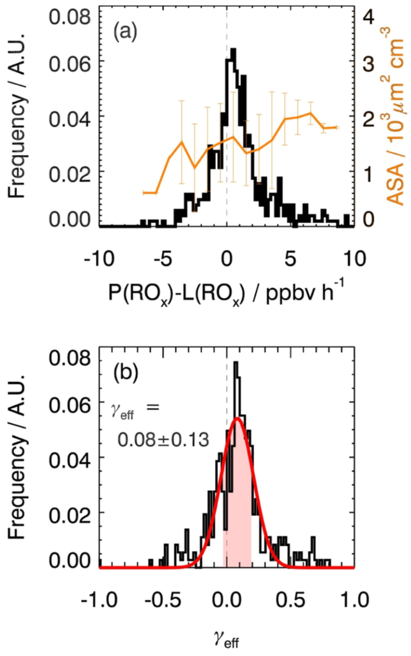

Figure 4. (a) Distributions of imbalances in the RO_x budget $(P - L)$ and the corresponding averaged ASA concentrations (vertical lines are standard deviations). (b) Distribution of calculated HO_2 uptake coefficients (eq 2). A fit to a Gaussian distribution (red line) yields a mean uptake coefficient of 0.08 and a standard deviation of 0.13 (1σ), indicated by the colored area. Data are selected from 08:00 to 16:00 to represent daytime conditions.

The HO_2 production rate is higher than its destruction rate, specifically in the morning hours. During this time of the day, high NO concentrations from traffic emissions enhance the

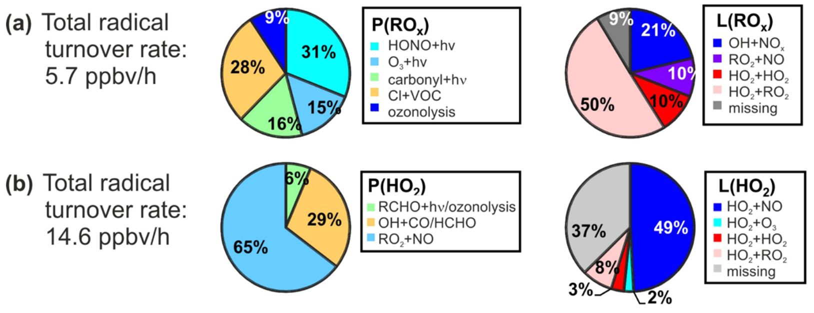

Figure 3. Relative contributions of single radical production and loss rates for RO_x (a) and HO_2 (b) during daytime (08:00−16:00). The contribution from $RO_2 + RO_2$ reactions to the total radical loss is <1% and is therefore not shown.

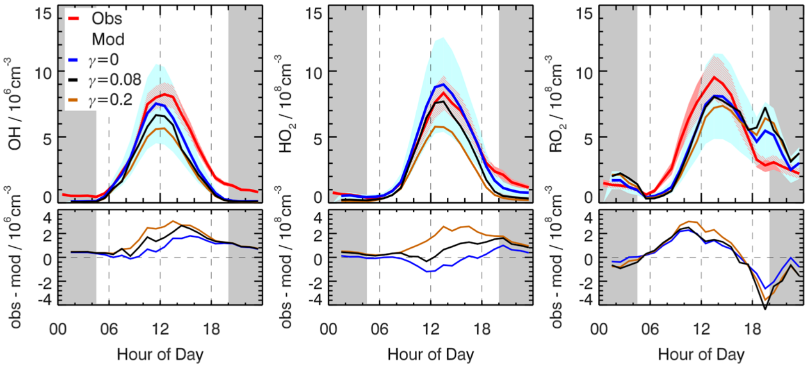

Figure 5. Mean diurnal profiles of observed and modeled OH, HO_2, and RO_2 radical concentrations during the campaign in Wangdu in 2014. Grey areas denote nighttime and colored areas denote $1 - \sigma$ deviations of the mean values of observations. Model results are shown without HO_2 uptake like in the previous analysis by Tan et al.[29] and with HO_2 uptake using an effective uptake coefficient of 0.2 used by Li et al. 2019 and of 0.08 determined as an upper limit in this work. The lower panels give the differences between observations and model calculations.

conversion of RO_2 to HO_2 radicals (Figures 2 and S5). The experimentally determined HO_2 production rate is higher than that in the model because model calculations tend to underestimate measured RO_2 concentrations under these conditions.[29] Maximum HO_2 production rates are up to 60 ppbv/h, much higher than maximum values of the RO_x production rate (Figure 2) because of the additional radical conversion reactions that cancel out in the RO_x budget. HO_2 production is on average 5.4 ± 0.5 ppbv/h (37 ± 10%) higher than its destruction (Figure 3b). In this case, the uncertainties in the nitrate yield and HO_2 + RO_2 reaction rate constants result in an uncertainty of 10% in the imbalance of the HO_2 budget because of the smaller contributions of these reactions to the total rates compared to the RO_x budget. The lower limit used for the organic nitrate yield of the reaction of RO_2 with NO could positively bias the HO_2 production rate because the competing reaction path leads to HO_2 formation. A higher nitrate yield would decrease the observed imbalance in the HO_2 budget. In contrast to the RO_x budget, the imbalance in the HO_2 budget is significantly indicating that not all loss processes are taken into account.

If HO_2 aerosol uptake was the loss process required to balance the HO_2 budget, the loss rate of the sum of radicals (RO_x) should increase by the same absolute amount. As a consequence, the total RO_x production rate would need to be twice as high compared to that of gas-phase sources calculated by measured precursors, if HO_2 uptake was the only unaccounted process, in order to balance the increased loss rate. This is much higher than the accuracy of the calculation and it appears unrealistic that such a high source of radicals (RO_x) is missed from processes that were not taken into account in the calculations (reactions S5−S10 and S18−S22). Therefore, an HO_2 loss process other than aerosol uptake is likely responsible for the observed imbalance in the average HO_2 budget. Thus, the imbalance of the RO_x budget represents an upper limit for potential HO_2 loss by uptake on aerosol.

The analysis of the RO_x radical budget suggests that there is not a missing loss process (Figures 4 and S5) such as HO_2 aerosol uptake within the uncertainty of the analysis (±1.3 ppbv/h, Supporting Information). However, it cannot be fully excluded that HO_2 aerosol uptake is balanced by an unaccounted radical production process. Such processes have been suggested for forested environments with high emissions from pine trees.[38,39] Because of the totally different emissions from vegetation and anthropogenic sources in Wangdu, it is unlikely that these results can be applied here.

There is a weak trend (Figure S6) of higher aerosol surface concentrations with increasing imbalance in the RO_x budget. However, values of imbalances occur only very infrequently, so that these values do not impact the averaged RO_x budget.

Although differences between production (P) and loss (L) rates in the RO_x budget are on average not significant (Figures 4 and S7), values can be used to estimate an HO_2 aerosol uptake coefficient that would be required to close the budget for each individual data point (derived from eq 1)

$$\gamma_{\mathrm{eff}} = \frac{P - L}{0.25 \cdot v_{\mathrm{HO_2}} \cdot [\mathrm{ASA}] \cdot [\mathrm{HO_2}]} \tag{2}$$

In this calculation, unphysical values can occur, for example, if $P - L$ is negative. The distribution of all calculated uptake coefficients (Figure 4b) can be fitted to a Gaussian distribution. The fit parameters can be attributed to an uptake coefficient of 0.08 ± 0.13 for conditions of the campaign.

In addition to the variability in the distribution from statistical errors, the uncertainties in the destruction and production rates add to the accuracies of the uptake coefficients. Taking maximum and minimum values within the error limits of P and L to calculate the HO_2 uptake coefficient would move the mean of the distribution to a range of −0.04 ± 0.11 and 0.19 ± 0.13. This demonstrates that the uptake coefficient can only be determined with high uncertainty from these measurements. The value depends on the content of TMIs such as copper Cu(I)/Cu(II) and iron Fe(II)/Fe(III) in the aerosol and the mixing state of the aerosol. A high TMI concentration (copper = 0.01 $\mu g/m^3$, iron = 0.12 $\mu g/m^3$, Table S1) would allow a high HO_2 uptake coefficient of 0.2 similar to values determined for filter samples taken at Mt. Mang and Mt. Tai in China.[20] However, the HO_2 uptake coefficient highly depends on the dissolved portion of TMIs[19] not determined here, so that lower values determined from the radical budget are possible.

Calculations using a chemical box model based on RACM2-LIM1[34,35] that does not include heterogeneous reactions[29] result in agreement within the uncertainties between modeled and observed radical concentrations (averaged diurnal profile) for most of the time (Figure 5). Specifically, the model−measurement agreement for HO_2 is excellent.

In a sensitivity test, HO_2 uptake is included in the model using the time series of ASA concentration measurements

(Supporting Information) and an effective uptake coefficient of 0.2 that was determined in previous studies[20] and is also used in the model studies by Li et al.[1,2]

Heterogeneous HO_2 uptake with a high uptake coefficient of 0.2 results in an additional radical loss of 1.4 ppbv/h and reduces the modeled HO_2 concentration on average by 40% during daytime (from 08:00 to 16:00). Only in late afternoon is the model−measurement discrepancy larger than the combined $1 - \sigma$ uncertainties,[29] in contrast to the good agreement without HO_2 uptake (Figure 5). The additional loss of HO_2 ($\gamma_{eff} = 0.2$) reduces also the modeled OH and RO_2 concentrations by 30 and 15%, respectively, at noontime. Modeled OH becomes significantly smaller than observations in the afternoon, whereas RO_2 shows a significant discrepancy in the morning. In summary, all radical species are less well-represented by the model, when HO_2 uptake with a high γ_{eff} value of 0.2 is included in the model. The impact of aerosol uptake on model results is much less, if an HO_2 uptake coefficient of 0.08 is applied. The difference between the model result with this value for the uptake coefficient and the model without aerosol uptake is only 17% for HO_2 concentrations.

The results of the analysis of imbalances in the radical production and destruction rates suggest that HO_2 uptake on aerosol did not play a role in determining peroxy radical concentrations and therefore also did not significantly affect the ozone production rate in the North China Plain in 2014. Conditions in the field campaign were representative for the North China Plain at that time (Supporting Information). In another campaign with no aerosol characterization conducted in Fall 2014 in the Pearl River Delta, the HO_2 and RO_x budget was also found to be closed,[36] suggesting again that HO_2 heterogeneous uptake was not important. Therefore, field observations of RO_x radicals do not support the hypothesis that HO_2 uptake was responsible for the increase of ozone in the North China Plain since 2014 (Figure S2).[1,2] Other reasons could be related to changes in the mix of anthropogenic emissions to a higher ratio of organic compounds to nitrogen oxides.[11−13]

■ ASSOCIATED CONTENT

Supporting Information

The Supporting Information is available free of charge at https://pubs.acs.org/doi/10.1021/acs.est.0c00525.

> Details of the calculation of radical production and destruction rates; description of particle properties; comparison of TMI measurements with other studies; summary of instrumentation; plot of the annual trend of O_3 and $PM_{2.5}$ concentrations in the North China Plain; plot of time series of NO, NO_2, and O_3; plot of the mean diurnal profiles of Cl_2 and $ClNO_2$; plot of the mean diurnal profiles of radical production and destruction rates; scatter plots of imbalance in the HO_2 budget and RO_x budget versus the ASA; scatter plot of $P(RO_x)$ versus $L(RO_x)$; and plots of the sensitivity of the differences between radical production and destruction rates with respect to organic nitrate yields (PDF)

■ AUTHOR INFORMATION

Corresponding Author

Hendrik Fuchs − *Institute of Energy and Climate Research, IEK-8: Troposphere, Forschungszentrum Jülich GmbH, 52428 Jülich, Germany; International Joint Laboratory for Regional Pollution Control, 52428 Jülich, Germany;* orcid.org/0000-0003-1263-0061; Phone: +49 2461 61 6741; Email: h.fuchs@fz-juelich.de

Authors

Zhaofeng Tan − *Institute of Energy and Climate Research, IEK-8: Troposphere, Forschungszentrum Jülich GmbH, 52428 Jülich, Germany; International Joint Laboratory for Regional Pollution Control, 52428 Jülich, Germany;* orcid.org/0000-0002-3808-1964

Andreas Hofzumahaus − *Institute of Energy and Climate Research, IEK-8: Troposphere, Forschungszentrum Jülich GmbH, 52428 Jülich, Germany; International Joint Laboratory for Regional Pollution Control, 52428 Jülich, Germany*

Keding Lu − *International Joint Laboratory for Regional Pollution Control, 52428 Jülich, Germany; State Key Joint Laboratory of Environmental Simulation and Pollution Control, College of Environmental Sciences and Engineering, Peking University, 100871 Beijing, China*

Steven S. Brown − *Chemical Sciences Division, NOAA Earth System Research Laboratory, Boulder, Colorado 80309, United States; Department of Chemistry, University of Colorado Boulder, Boulder, Colorado 80309, United States*

Frank Holland − *Institute of Energy and Climate Research, IEK-8: Troposphere, Forschungszentrum Jülich GmbH, 52428 Jülich, Germany; International Joint Laboratory for Regional Pollution Control, 52428 Jülich, Germany*

Lewis Gregory Huey − *School of Earth and Atmospheric Sciences, Georgia Institute of Technology, Atlanta, Georgia 30332, United States;* orcid.org/0000-0002-0518-7690

Astrid Kiendler-Scharr − *Institute of Energy and Climate Research, IEK-8: Troposphere, Forschungszentrum Jülich GmbH, 52428 Jülich, Germany; International Joint Laboratory for Regional Pollution Control, 52428 Jülich, Germany*

Xin Li − *International Joint Laboratory for Regional Pollution Control, 52428 Jülich, Germany; State Key Joint Laboratory of Environmental Simulation and Pollution Control, College of Environmental Sciences and Engineering, Peking University, 100871 Beijing, China;* orcid.org/0000-0001-5129-4801

Xiaoxi Liu − *School of Earth and Atmospheric Sciences, Georgia Institute of Technology, Atlanta, Georgia 30332, United States;* orcid.org/0000-0002-5104-8886

Nan Ma − *Leibniz Institute for Tropospheric Research, 04318 Leipzig, Germany*

Kyung-Eun Min − *Cooperative Institute for Research in Environmental Sciences, University of Colorado Boulder, Boulder, Colorado 80309, United States*

Franz Rohrer − *Institute of Energy and Climate Research, IEK-8: Troposphere, Forschungszentrum Jülich GmbH, 52428 Jülich, Germany; International Joint Laboratory for Regional Pollution Control, 52428 Jülich, Germany*

Min Shao − *International Joint Laboratory for Regional Pollution Control, 52428 Jülich, Germany; State Key Joint Laboratory of Environmental Simulation and Pollution Control, College of Environmental Sciences and Engineering, Peking University, 100871 Beijing, China*

Andreas Wahner − *Institute of Energy and Climate Research, IEK-8: Troposphere, Forschungszentrum Jülich GmbH, 52428 Jülich, Germany; International Joint Laboratory for Regional Pollution Control, 52428 Jülich, Germany*

Yuhang Wang − *School of Earth and Atmospheric Sciences, Georgia Institute of Technology, Atlanta, Georgia 30332, United States*

Alfred Wiedensohler − *Leibniz Institute for Tropospheric Research, 04318 Leipzig, Germany*

Yusheng Wu − *State Key Joint Laboratory of Environmental Simulation and Pollution Control, College of Environmental Sciences and Engineering, Peking University, 100871 Beijing, China*

Zhijun Wu − *International Joint Laboratory for Regional Pollution Control, 52428 Jülich, Germany; State Key Joint Laboratory of Environmental Simulation and Pollution Control, College of Environmental Sciences and Engineering, Peking University, 100871 Beijing, China;* orcid.org/0000-0001-8910-5674

Limin Zeng − *International Joint Laboratory for Regional Pollution Control, 52428 Jülich, Germany; State Key Joint Laboratory of Environmental Simulation and Pollution Control, College of Environmental Sciences and Engineering, Peking University, 100871 Beijing, China*

Yuanhang Zhang − *International Joint Laboratory for Regional Pollution Control, 52428 Jülich, Germany; State Key Joint Laboratory of Environmental Simulation and Pollution Control, College of Environmental Sciences and Engineering and Beijing Innovation Center for Engineering Science and Advanced Technology, Peking University, 100871 Beijing, China; CAS Center for Excellence in Regional Atmospheric Environment, Chinese Academy of Science, 361000 Xiamen, China*

Complete contact information is available at:
https://pubs.acs.org/10.1021/acs.est.0c00525

Notes

The authors declare no competing financial interest.

ACKNOWLEDGMENTS

We thank the science team of the campaign in Wangdu 2014 for supporting the field campaign. This research has received funding from the National Natural Science Foundation of China (grant nos. 21522701, 91544225, 21190052, and 41375124), the Collaborative Innovation Center for Regional Environmental Quality, the Bundesministerium für Bildung, Wissenschaft, Forschung und Technologie, Germany, project ID-CLAR (grant agreement no. 01DO17036), the European Commission's FP7 People project AMIS (grant agreement no. PIRSES-GA-2011-295132), and the European Commissions's Horizon 2020 ERC project SARLEP (grant agreement no. 681529).

REFERENCES

(1) Li, K.; Jacob, D. J.; Liao, H.; Shen, L.; Zhang, Q.; Bates, K. H. Anthropogenic drivers of 2013-2017 trends in summer surface ozone in China. *Proc. Natl. Acad. Sci. U.S.A.* **2019**, *116*, 422−427.

(2) Li, K.; Jacob, D. J.; Liao, H.; Zhu, J.; Shah, V.; Shen, L.; Bates, K. H.; Zhang, Q.; Zhai, S. A two-pollutant strategy for improving ozone and particulate air quality in China. *Nat. Geosci.* **2019**, *12*, 906−910.

(3) Lu, X.; Hong, J.; Zhang, L.; Cooper, O. R.; Schultz, M. G.; Xu, X.; Wang, T.; Gao, M.; Zhao, Y.; Zhang, Y. Severe surface ozone pollution in China: A Global Perspective. *Environ. Sci. Technol. Lett.* **2018**, *5*, 487−494.

(4) Li, J.; Lu, K.; Lv, W.; Li, J.; Zhong, L.; Ou, Y.; Chen, D.; Huang, X.; Zhang, Y. Fast increasing of surface ozone concentrations in Pearl River Delta characterized by a regional air quality monitoring network during 2006-2011. *J. Environ. Sci.* **2014**, *26*, 23−36.

(5) Wang, W.-N.; Cheng, T.-H.; Gu, X.-F.; Chen, H.; Guo, H.; Wang, Y.; Bao, F.-W.; Shi, S.-Y.; Xu, B.-R.; Zuo, X.; Meng, C.; Zhang, X.-C. Assessing spatial and temporal patterns of observed ground-level ozone in China. *Sci. Rep.* **2017**, *7*, 3651.

(6) Yeung, L. Y.; Murray, L. T.; Martinerie, P.; Witrant, E.; Hu, H.; Banerjee, A.; Orsi, A.; Chappellaz, J. Isotopic constraint on the twentieth-century increase in tropospheric ozone. *Nature* **2019**, *570*, 224−227.

(7) Parrish, D. D.; Young, L. M.; Newman, M. H.; Aikin, K. C.; Ryerson, T. B. Ozone design values in Southern California's air basins: Temporal evolution and U.S. background contribution. *J. Geophys. Res.* **2017**, *122*, 11166−11182.

(8) Wang, T.; Wei, X. L.; Ding, A. J.; Poon, C. N.; Lam, K. S.; Li, Y. S.; Chan, L. Y.; Anson, M. Increasing surface ozone concentrations in the background atmosphere of Southern China, 1994−2007. *Atmos. Chem. Phys.* **2009**, *9*, 6217−6227.

(9) Geng, F.; Mao, X.; Zhou, M.; Zhong, S.; Lenschow, D. Multi-year ozone concentration and its spectra in Shanghai, China. *Sci. Total Environ.* **2015**, *521-522*, 135−143.

(10) Sun, L.; Xue, L.; Wang, Y.; Li, L.; Lin, J.; Ni, R.; Yan, Y.; Chen, L.; Li, J.; Zhang, Q.; Wang, W. Impacts of meteorology and emissions on summertime surface ozone increases over central eastern China between 2003 and 2015. *Atmos. Chem. Phys.* **2019**, *19*, 1455−1469.

(11) Sun, L.; Xue, L.; Wang, T.; Gao, J.; Ding, A.; Cooper, O. R.; Lin, M.; Xu, P.; Wang, Z.; Wang, X.; Wen, L.; Zhu, Y.; Chen, T.; Yang, L.; Wang, Y.; Chen, J.; Wang, W. Significant increase of summertime ozone at Mount Tai in Central Eastern China. *Atmos. Chem. Phys.* **2016**, *16*, 10637−10650.

(12) Zhang, Q.; Yuan, B.; Shao, M.; Wang, X.; Lu, S.; Lu, K.; Wang, M.; Chen, L.; Chang, C.-C.; Liu, S. C. Variations of ground-level O_3 and its precursors in Beijing in summertime between 2005 and 2011. *Atmos. Chem. Phys.* **2014**, *14*, 6089−6101.

(13) Liu, X.; Lyu, X.; Wang, Y.; Jiang, F.; Guo, H. Intercomparison of O_3 formation and radical chemistry in the past decade at a suburban site in Hong Kong. *Atmos. Chem. Phys.* **2019**, *19*, 5127−5145.

(14) Shao, M.; Zhang, Y.; Zeng, L.; Tang, X.; Zhang, J.; Zhong, L.; Wang, B. Ground-level ozone in the Pearl River Delta and the roles of VOC and NO(x) in its production. *J. Environ. Manage.* **2009**, *90*, 512−518.

(15) Zhang, Y. H.; Su, H.; Zhong, L. J.; Cheng, Y. F.; Zeng, L. M.; Wang, X. S.; Xiang, Y. R.; Wang, J. L.; Gao, D. F.; Shao, M.; Fan, S. J.; Liu, S. C. Regional ozone pollution and observation-based approach for analyzing ozone−precursor relationship during the PRIDE-PRD2004 campaign. *Atmos. Environ.* **2008**, *42*, 6203−6218.

(16) Tan, Z.; Lu, K.; Jiang, M.; Su, R.; Dong, H.; Zeng, L.; Xie, S.; Tan, Q.; Zhang, Y. Exploring ozone pollution in Chengdu, southwestern China: A case study from radical chemistry to O_3-VOC-NO_x sensitivity. *Sci. Total Environ.* **2018**, *636*, 775−786.

(17) Tan, Z.; Lu, K.; Jiang, M.; Su, R.; Wang, H.; Lou, S.; Fu, Q.; Zhai, C.; Tan, Q.; Yue, D.; Chen, D.; Wang, Z.; Xie, S.; Zeng, L.; Zhang, Y. Daytime atmospheric oxidation capacity in four Chinese megacities during the photochemically polluted season: a case study based on box model simulation. *Atmos. Chem. Phys.* **2019**, *19*, 3493−3513.

(18) Jacob, D. Heterogeneous chemistry and tropospheric ozone. *Atmos. Environ.* **2000**, *34*, 2131−2159.

(19) Mao, J.; Fan, S.; Jacob, D. J.; Travis, K. R. Radical loss in the atmosphere from Cu-Fe redox coupling in aerosols. *Atmos. Chem. Phys.* **2013**, *13*, 509−519.

(20) Taketani, F.; Kanaya, Y.; Pochanart, P.; Liu, Y.; Li, J.; Okuzawa, K.; Kawamura, K.; Wang, Z.; Akimoto, H. Measurement of overall uptake coefficients for HO_2 radicals by aerosol particles sampled from ambient air at Mts. Tai and Mang (China). *Atmos. Chem. Phys.* **2012**, *12*, 11907−11916.

(21) Thornton, J. A.; Jaegle, L.; McNeill, V. F. Assessing known pathways for HO_2 loss in aqueous atmospheric aerosols: Regional and global impacts on tropospheric oxidants. *J. Geophys. Res.* **2008**, *113*, D05303.

(22) Mozurkewich, M.; McMurry, P. H.; Gupta, A.; Calvert, J. G. Mass accommodation coefficient for HO_2 radicals on aqueous particles. *J. Geophys. Res.: Atmos.* **1987**, *92*, 4163−4170.

(23) George, I. J.; Vlasenko, A.; Slowik, J. G.; Broekhuizen, K.; Abbatt, J. P. D. Heterogeneous oxidation of saturated organic aerosols by hydroxyl radicals: uptake kinetics, condensed-phase products, and particle size change. *Atmos. Chem. Phys.* **2007**, *7*, 4187−4201.

(24) Lakey, P. S. J.; George, I. J.; Whalley, L. K.; Baeza-Romero, M. T.; Heard, D. E. Measurements of the HO_2 uptake coefficients onto single component organic aerosols. *Environ. Sci. Technol.* **2015**, *49*, 4878−4885.

(25) George, I. J.; Matthews, P. S. J.; Whalley, L. K.; Brooks, B.; Goddard, A.; Baeza-Romero, M. T.; Heard, D. E. Measurements of uptake coefficients for heterogeneous loss of HO_2 onto submicron inorganic salt aerosols. *Phys. Chem. Chem. Phys.* **2013**, *15*, 12829−12845.

(26) Taketani, F.; Kanaya, Y.; Akimoto, H. Heterogeneous loss of HO_2 by KCl, synthetic sea salt, and natural seawater aerosol particles. *Atmos. Environ.* **2009**, *43*, 1660−1665.

(27) Taketani, F.; Kanaya, Y.; Akimoto, H. Kinetics of heterogeneous reactions of HO_2 radical at ambient concentration levels with $(NH_4)_2SO_4$ and NaCl aerosol particles. *J. Phys. Chem. A* **2008**, *112*, 2370−2377.

(28) Taketani, F.; Kanaya, Y.; Akimoto, H. Kinetics of HO_2 uptake in levoglucosan and polystyrene latex particles. *J. Phys. Chem. Lett.* **2010**, *1*, 1701−1704.

(29) Tan, Z.; Fuchs, H.; Lu, K.; Hofzumahaus, A.; Bohn, B.; Broch, S.; Dong, H.; Gomm, S.; Häseler, R.; He, L.; Holland, F.; Li, X.; Liu, Y.; Lu, S.; Rohrer, F.; Shao, M.; Wang, B.; Wang, M.; Wu, Y.; Zeng, L.; Zhang, Y.; Wahner, A.; Zhang, Y. Radical chemistry at a rural site (Wangdu) in the North China Plain: observation and model calculations of OH, HO_2 and RO_2 radicals. *Atmos. Chem. Phys.* **2017**, *17*, 663−690.

(30) Fuchs, H.; Tan, Z.; Lu, K.; Bohn, B.; Broch, S.; Brown, S. S.; Dong, H.; Gomm, S.; Häseler, R.; He, L.; Hofzumahaus, A.; Holland, F.; Li, X.; Liu, Y.; Lu, S.; Min, K.-E.; Rohrer, F.; Shao, M.; Wang, B.; Wang, M.; Wu, Y.; Zeng, L.; Zhang, Y.; Wahner, A.; Zhang, Y. OH reactivity at a rural site (Wangdu) in the North China Plain: contributions from OH reactants and experimental OH budget. *Atmos. Chem. Phys.* **2017**, *17*, 645−661.

(31) Wang, Y.; Chen, Z.; Wu, Q.; Liang, H.; Huang, L.; Li, H.; Lu, K.; Wu, Y.; Dong, H.; Zeng, L.; Zhang, Y. Observation of atmospheric peroxides during Wangdu Campaign 2014 at a rural site in the North China Plain. *Atmos. Chem. Phys.* **2016**, *16*, 10985−11000.

(32) Tham, Y. J.; Wang, Z.; Li, Q.; Yun, H.; Wang, W.; Wang, X.; Xue, L.; Lu, K.; Ma, N.; Bohn, B.; Li, X.; Kecorius, S.; Größ, J.; Shao, M.; Wiedensohler, A.; Zhang, Y.; Wang, T. Significant concentrations of nitryl chloride sustained in the morning: investigations of the causes and impacts on ozone production in a polluted region of northern China. *Atmos. Chem. Phys.* **2016**, *16*, 14959−14977.

(33) Liu, X.; Qu, H.; Huey, L. G.; Wang, Y.; Sjostedt, S.; Zeng, L.; Lu, K.; Wu, Y.; Hu, M.; Shao, M.; Zhu, T.; Zhang, Y. High levels of daytime molecular chlorine and nitryl chloride at a rural site on the North China Plain. *Environ. Sci. Technol.* **2017**, *51*, 9588−9595.

(34) Goliff, W. S.; Stockwell, W. R.; Lawson, C. V. The regional atmospheric chemistry mechanism, version 2. *Atmos. Environ.* **2013**, *68*, 174−185.

(35) Peeters, J.; Müller, J.-F.; Stavrakou, T.; Nguyen, V. S. Hydroxyl radical recycling in isoprene oxidation driven by hydrogen bonding and hydrogen tunneling: The upgraded LIM1 mechanism. *J. Phys. Chem. A* **2014**, *118*, 8625−8643.

(36) Tan, Z.; Lu, K.; Hofzumahaus, A.; Fuchs, H.; Bohn, B.; Holland, F.; Liu, Y.; Rohrer, F.; Shao, M.; Sun, K.; Wu, Y.; Zeng, L.; Zhang, Y.; Zou, Q.; Kiendler-Scharr, A.; Wahner, A.; Zhang, Y. Experimental budgets of OH, HO_2, and RO_2 radicals and implications for ozone formation in the Pearl River Delta in China 2014. *Atmos. Chem. Phys.* **2019**, *19*, 7129−7150.

(37) Jenkin, M. E.; Valorso, R.; Aumont, B.; Rickard, A. R. Estimation of rate coefficients and branching ratios for reactions of organic peroxy radicals for use in automated mechanism construction. *Atmos. Chem. Phys.* **2019**, *19*, 7691−7717.

(38) Wolfe, G. M.; Cantrell, C.; Kim, S.; Mauldin Iii, R. L.; Karl, T.; Harley, P.; Turnipseed, A.; Zheng, W.; Flocke, F.; Apel, E. C.; Hornbrook, R. S.; Hall, S. R.; Ullmann, K.; Henry, S. B.; DiGangi, J. P.; Boyle, E. S.; Kaser, L.; Schnitzhofer, R.; Hansel, A.; Graus, M.; Nakashima, Y.; Kajii, Y.; Guenther, A.; Keutsch, F. N. Missing peroxy radical sources within a summertime ponderosa pine forest. *Atmos. Chem. Phys.* **2014**, *14*, 4715−4732.

(39) Hens, K.; Novelli, A.; Martinez, M.; Auld, J.; Axinte, R.; Bohn, B.; Fischer, H.; Keronen, P.; Kubistin, D.; Nölscher, A. C.; Oswald, R.; Paasonen, P.; Petäjä, T.; Regelin, E.; Sander, R.; Sinha, V.; Sipilä, M.; Taraborrelli, D.; Tatum Ernest, C.; Williams, J.; Lelieveld, J.; Harder, H. Observation and modelling of HO_X radicals in a boreal forest. *Atmos. Chem. Phys.* **2014**, *14*, 8723−8747.

https://dx.doi.org/10.1021/acs.est.0c00525